SWRI/LASP SOUNDING ROCKET INTER-CALIBRATION WITH THE EIT INSTRUMENT ON BOARD SOHO

FRÉDÉRIC AUCHÈRE[1], DONALD M. HASSLER[2], DAVID C. SLATER[2] and THOMAS N. WOODS[3]
[1] *USRA/NASA/GSFC, Code 682.3, Building 26, Room G-1, Greenbelt, MD 20771, U.S.A.*
[2] *Southwest Research Institute, 1050 Walnut St., Suite 426, Boulder, CO 80302, U.S.A.*
[3] *University of Colorado/LASP, Boulder, CO 80307, U.S.A.*

(Received 7 March 2001; accepted 10 May 2001)

Abstract. Two successful sounding rocket flights were launched on 15 May 1997 and 2 November 1998 with an objective of providing inter-calibration with several of the instruments on board SOHO and TRACE. We will discuss here the results of the inter-calibration between the SwRI/LASP rocket imaging instruments and the Extreme-ultraviolet Imaging Telescope (EIT) on SOHO. The Multiple XUV Imager (MXUVI) sounding rocket instrument is a multi-layer mirror telescope equipped with an internal occulter and light trap to provide full-disk images of Fe IX/X 17.1 nm and off-limb observations of He II 30.4 nm. The SOHO/EIT instrument is also a full-disk multi-layer imager with four channels, Fe IX/X 17.1 nm, Fe XII 19.5 nm, Fe XV 28.4 nm and He II 30.4 nm. By comparison with the EIT observations taken at the same time, we provide new flat-field determinations for EIT which help quantify the sensitivity degradation of the EIT detector, as well as provide a measure of the off-limb stray-light characteristics of the two instruments. We find that the EIT stray-light function is strongly asymmetric, with greater stray light in the 17.1 and 19.5 nm quadrants than the 30.4 and 28.4 nm quadrants. Two possible causes of this asymmetry are the polishing processes of the EIT mirrors and the asymmetric support grid pattern in the foil mesh at the EIT pupil.

1. Introduction

If a well-calibrated instrument observes the Sun simultaneously with an uncalibrated instrument, then the comparison of their observations allows one to deduce some of the calibration parameters of the second instrument. The EIT CalRoc (Defise, Moses, and Clette, 1998a) sounding rocket of 16 October 1997 was launched with the objective to calibrate the Extreme-ultraviolet Imaging Telescope (EIT) on board the Solar and Heliospheric Observatory (Domingo, Fleck, and Poland, 1995) (SOHO), but since the rocket instrument was an exact copy of the EIT, fundamental parameters such as the stray-light function were identical in the two instruments and thus impossible to evaluate. During two sounding rocket flights on 15 May 1997 and 2 November 1998 the SwRI/LASP Multiple XUV Imager (MXUVI) instrument provided good quality images of the EUV solar corona, useful for inter-calibration purposes with the EIT. Since these instruments are completely different, no instrumental effects are expected to be identical. Because of this,

Solar Physics **202:** 269–280, 2001.

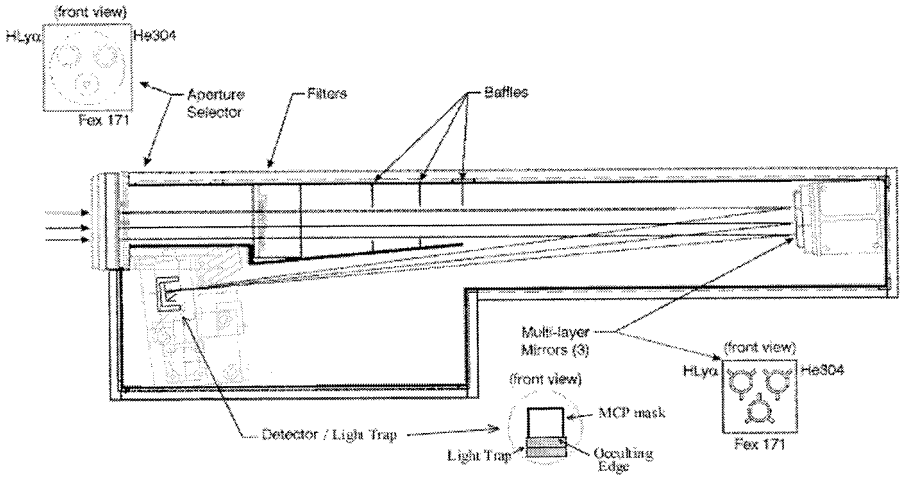

Figure 1. Optical layout of the MXUVI instrument. An aperture selector illuminates in sequential order one of three multi-layer telescope mirrors incident on the same detector. Solar disk radiation from the H I Lyα and He II 304 channels is centered on an internal light trap inside the detector housing (below the plane of the drawing), while full-disk images from the Fe X 171 channel are incident directly on the MCP.

MXUVI provided both flat-fields for EIT, and provided valuable information about the stray-light function of the EIT, a critical parameter in the data reduction process.

1.1. THE MXUVI INSTRUMENT

The Multiple XUV Imager (MXUVI), shown in Figure 1, consists of an aperture selector and three small telescope mirrors (750 mm focal length) which form an image of the Sun on a 256 × 256 CODACON detector with 10 × 10 arc sec image pixel size. The aperture selector illuminates in sequential order one of the three multi-layer mirrors on the detector. For the two coronal channels, the imager is equipped with a special internal occulter, light trap and baffles to discard unwanted disk radiation and prevent scattered disk light from reaching the MCP detector and saturating the coronal signal. Two of the three telescope mirrors have Mo/Si multilayer coatings with narrow band passes (Dl/l = 0.1) peaked at 30.4 nm and 17.1 nm. For the 15 May 1997 flight (NASA 36.135), these mirrors were coated by the same laboratory (Dr Chauvineau, Institut d'Optique in Orsay, France) as the EIT telescope mirrors on the SOHO satellite. For the 2 November 1998 flight (NASA 36.171), super-polished (0.5 Å r.m.s.) substrates were coated by Dr Troy Barbee at Lawrence Livermore National Laboratory (LLNL). The third mirror has an Al/MgF2 coating with peak transmission near 121.6 nm. Combinations of thin Al/Si and Al/Lexan filters and an interference filter (121.6 nm) are placed in the aperture selector to isolate the wavelength regions for each telescope mirror. Solar disk radiation from the H I Ly-alpha and He II 304 channels is centered on an internal light trap inside the detector housing (below the plane of the drawing in

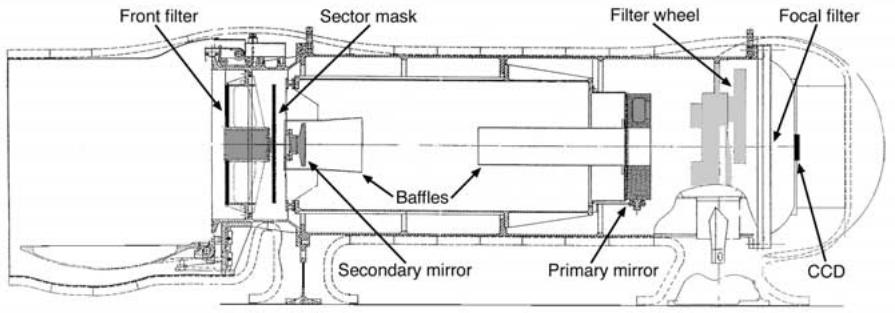

Figure 2. Optical layout of the EIT instrument.

Figure 1), while full-disk images from the Fe X 171 channel are incident directly on the detector. The aperture selector is a prototype of the TIMED/Solar EUV Experiment (SEE; Tom Woods, PI) filter wheel mechanism, utilizing an eight position Geneva mechanism design. During flight, the aperture or channel selection is made via a real-time telemetry uplink so that the integration time per wavelength is optimized.

1.2. THE EIT INSTRUMENT

The EIT (Delaboudinière *et al.*, 1995) has provided full-disk EUV images of the solar corona continuously since early 1996, as part of the SOHO scientific payload. Figure 2 is a side view showing the internal configuration of the instrument. It is a Ritchey–Chrétien telescope whose primary and secondary mirrors are coated with multilayer deposits to define four quadrants isolating four narrow pass bands of the extreme ultraviolet spectrum : 17.1 nm (Fe IX/Fe X), 19.5 nm (Fe XII), 28.4 nm (Fe XV), 30.4 nm (Si XI/He II). The white-light radiation is suppressed by the aluminum 'front filter' and 'focal filter'. Extra aluminum filters can be added in the optical path with the 'filter wheel'. The 'sector mask' selects one of the four quadrants at a time. The photons are detected by a backside illuminated CCD of 1024 by 1024 pixels, offering a maximum resolution of 2.629 arc sec pixel^{-1} (Auchère, DeForest, and Artzner, 2000) and a 14000 Digital Numbers (DN) dynamic range. Although calibrated before flight (Dere *et al.*, 2000) the response of the EIT varies with time, hence the need of an in-flight calibration.

1.3. OBSERVATIONS

During the two rocket flights, the MXUVI took on-disk images at 17.1 nm and off-disk images between one and three solar radii at 30.4 nm. Different off-disk pointing positions and roll angles were used to cover a wider area of the corona and to check the level of scattered light. The MXUVI is equipped with a photon-counting detector, allowing short exposure times of a few seconds so that during the typically five usable minutes of each sounding rocket flight, more than a hundred

images could be recorded. At the same time, the EIT took 5.2 arc sec resolution images in all four wavelengths with a 2 min cadence. As a result, there is a maximum time difference of 2 min between the MXUVI and the EIT images.

1.4. Data reduction

After the flights, we co-added the MXUVI images from each flight into a single image for each pointing position. A repeller grid used to improve detector quantum efficiency is located in front of the detector of the MXUVI and creates a shadow pattern composed of horizontal and diagonal lines. To remove it from the co-added images, we used a semi-automatic pattern-recognition algorithm, and then rescaled the corresponding pixels to the average of their closest neighbors. The degrided images were then flat-fielded with laboratory flat-fields. The laboratory flat-field images are composed of low-amplitude small scale variations superimposed to a global trend. We then used a bilinear fit that removes the global trend but does not correct for the small scale variations. Finally the resulting images for each pointing position were coaligned and co-added together. The summed rocket images were then co-aligned with the most recent EIT images. The coalignments were made using the pointing information contained in the telemetry, in combination with limb-fitting and cross-correlation algorithms. The stray-light function is the only unknown instrumental effect. For the EIT images, we applied the degriding, devignetting and background subtraction, and we degraded them to match the MXUVI resolution. The uncorrected parameters are the flat-field and the stray-light function.

1.5. Calibration issues

Figure 3 shows the final preprocessed MXUVI images at 17.1 nm for the two flights, along with the simultaneous EIT observations. Figure 4 shows the final 30.4 nm MXUVI images composited with the corresponding EIT images. In both figures, the observations made by the two instruments are very similar, but slight differences reveal inter-calibration problems. At 17.1 nm, the contrast between the disk and the corona is different between the EIT and MXUVI images because the stray-light levels are different in the two instruments, and the EIT CCD is degraded on disk. This degradation also causes the dark ring around the limb in the 30.4 nm EIT images (especially in 1997, see arrow 1). The match between the EIT and the MXUVI image in 1997 is good, except for one small discontinuity (arrow 2). In 1998, the MXUVI and EIT coronal images at 30.4 nm matched only roughly (see the steps marked by the arrows 3 and 4), because of the significantly lower stray-light level for MXUVI during that flight. In the next sections, we describe how appropriate processing permits us to extract the flat-field of the EIT and to understand the stray-light levels in the two instruments.

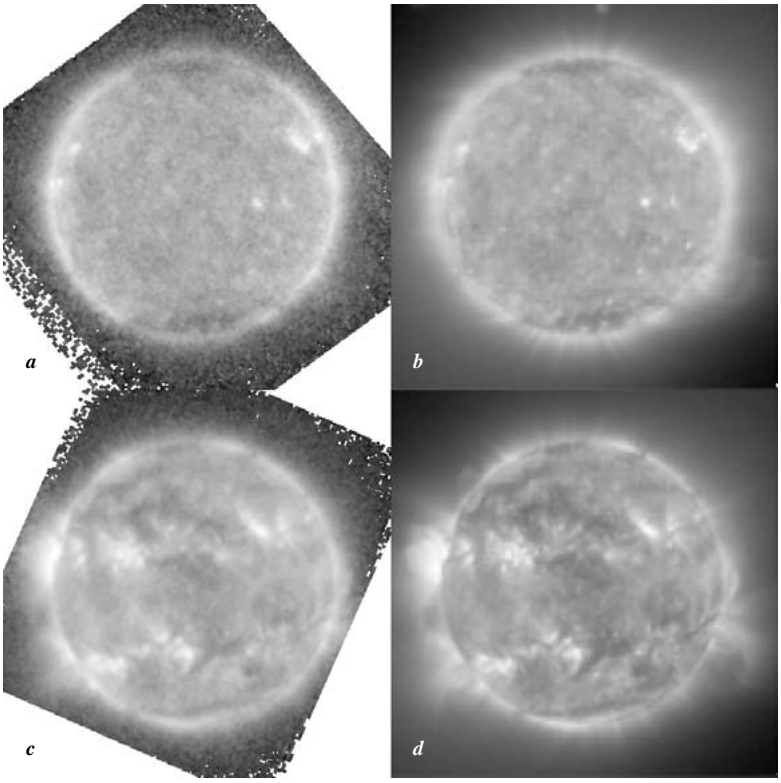

Figure 3. Observations at 17.1 nm. (a) The final co-added MXUVI image of 15 May 1997. (b) The corresponding EIT image. (c) The final co-added MXUVI image of 2 November 1998. (d) The corresponding EIT image. Except for the lower signal-to-noise ratio of the MXUVI images, the MXUVI and EIT observations are very similar.

2. Flat-Fielding of the EIT

Figure 5 is a plot of the average count rate per unit time in the full-field EIT 30.4 nm images from the beginning of the operations. The decreases reveal a degradation of the detector. The sharp increases are caused by the regular bake-outs of the CCD performed to recover part of its nominal response. As shown by Defise *et al.* (1998) the loss of sensitivity between two bake-outs has two different origins. First, the condensation on the CCD of the residual water vapor creates a thin absorbing layer of ice. Second, the EUV radiation causes photochemical reactions inside the detector structure that affect the charge collection efficiency itself. Since the degradation due to EUV radiation is not uniform, and since EIT has no on-board EUV flat-fielding, it is impossible to correct the images.

The two rocket flights of the MXUVI were good opportunities to estimate the level of degradation of the EIT CCD. After the preprocessing, the signal in the MXUVI images is simply the convolution of the incident signal with the stray-light

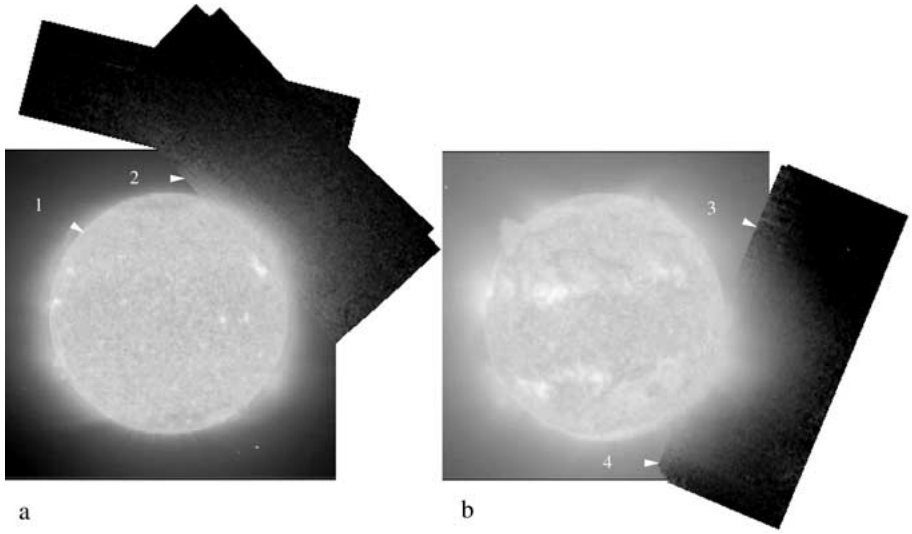

Figure 4. Observations at 30.4 nm. (a) The final co-added MXUVI image of 15 May 1997 superposed with the corresponding EIT image. (b) The final co-added MXUVI image of 2 November 1998 superposed with the corresponding EIT image. Subtle differences marked by the arrows reveal the absence of flat-fielding of the EIT and the different stray-light levels in the two instruments. For example, the 1998 mosaic shows obvious discontinuities (see arrows 3, 4), because the MXUVI had a much lower stray-light level than the EIT during that flight.

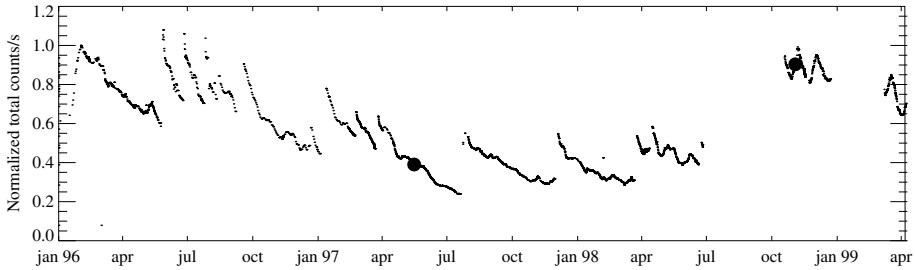

Figure 5. Average count rate per unit time in full-field EIT 30.4 nm images from the beginning of operation. The global decrease is due to the aging of the EIT CCD. The sharp increases are due to the bake-outs performed to restore part of its original sensitivity. The two spots mark the degradation level at the dates of two rocket flights.

function. In the case of the EIT, the signal is furthermore multiplied by the flat-field. Assuming that the pass bands of the the two instruments are identical, the ratios of Figure 6 between the MXUVI and EIT images (Figure 3(a) over Figure 3(b) for 1997 and Figure 3(c) over by Figure 3(d) for 1998) are therefore EIT flat-fields multiplied by a function of the stray-light levels in the two instruments. Since these maps depend on two different instrumental effects, their interpretation is not straightforward, but by exploiting some characteristics of the data we can separate the information relative to the flat-fields from the information relative to the stray-

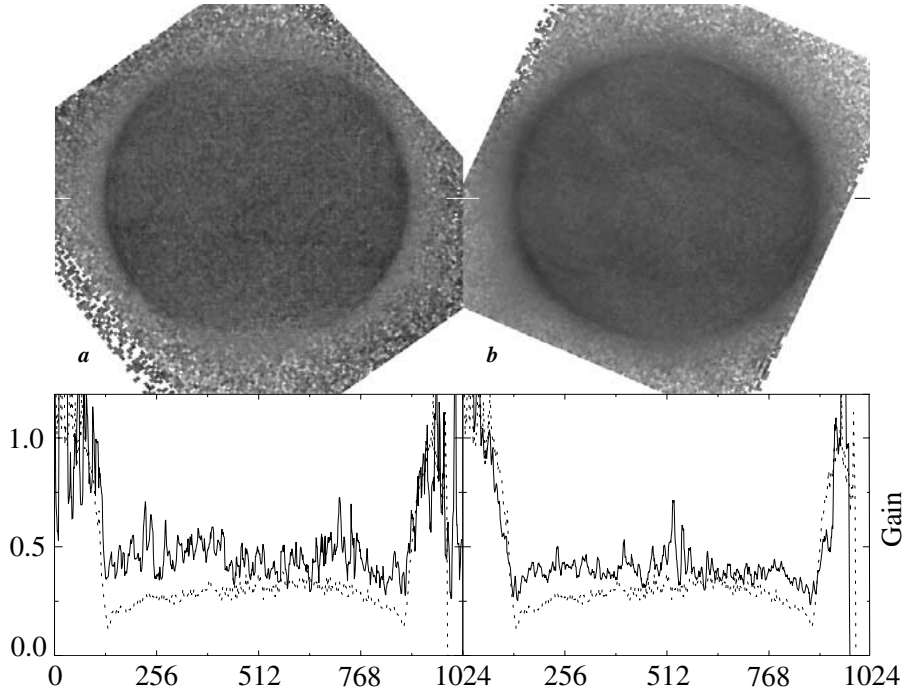

Figure 6. Ratios of the images Figure 3. (a) For 1997, (b) for 1998 – along with equatorial cuts (*solid lines*). For comparisons, the gain extracted from the CalRoc data is plotted in *dashed lines*. Because the stray-light levels of the EIT and of the MXUVI are different, each image contains information on both the EIT flat-field and the stray-light levels in the two instruments.

light. On-disk and off-disk below 1.2 solar radii, where the incident signal is strong and the contribution of the scattered light is negligible, the ratios are true flat-fields of the EIT CCD. Higher in the corona the degradation of the EIT detector is small and almost uniform (see Defise *et al.*, 1998), and the ratios there are functions of the stray-light levels only. We will discuss this latter aspect in the next section. Since the absolute calibrations of the two instruments are not better than 20%, the flat-fields are determined only to within a multiplicative constant. The two equatorial cuts of Figure 6 are therefore arbitrarily scaled to 1 in the corners of the field of view where the degradation is supposed to be negligible. Below 1.2 solar radii, both ratios show an average negative image of the Sun imprinted in the EIT CCD. This is expected since part of the degradation is a function of the total EUV dose. The surrounding dark ring corresponds to the limb brightening. The polar regions are less degraded than the rest of the disk because of the lower EUV flux in the coronal holes. In the 1998 ratio, the rising solar activity results in a strong degradation at the latitude of the active regions belts. These flat-fields are consistent in shape with those extracted from the EIT/CalRoc data (represented by the dashed lines in Figure 6), although the absolute values are different because they correspond to a different time in the CCD's aging history.

The resolution of these flat-fields is only as good as the MXUVI resolution and therefore can only be used to correct for large-scale variations across the detector. Also, due to the rapid evolution of the CCD degradation they are usable only for a limited period of time. But like the flat-fields extracted from the CalRoc data they provide good constraints for the aging models of the EIT CCD, which help to deduce the degradation from the total EUV dose history.

3. Stray-Light Levels

The knowledge of the stray-light level is critical for off-disk observations, because the weak coronal signal can be contaminated by instrumentally scattered disk radiation. Unfortunately the stray-light function of the EIT has never been satisfactorily estimated. Some observations of bright active regions showed that the pre-flight measurements strongly overestimated the wings of the EIT stray-light profile. Since the CalRoc is an exact copy of the EIT and even used the spare EIT mirrors, the stray-light levels were identical in the two instruments and therefore cancelled out in the analysis. Since the MXUVI has a completely different optical design, its stray-light function is not expected to be the same as for EIT. The MXUVI was equipped with two different sets of mirrors in 1997 and 1998, the second set being smoother (0.5 Å r.m.s.) and therefore less scattering. For EIT, the stray-light level is expected to be the same for the two dates. From the CalRoc data, we know that the EIT detector is only slightly degraded off disk, and that the flat-fields are very similar in the four EIT pass bands. Since the ratios of 17.1 nm images give the flat-field of the EIT, we can also use them to correct the 30.4 nm EIT images below 1.2 solar radii. As a result, the ratios in Figure 7 between the 30.4 nm EIT and MXUVI images are functions of the stray-light level ratios in the two instruments.

The 1997 ratio is pretty uniform, meaning that the stray-light levels were similar in the EIT and in the MXUVI. The bright features are residual random patterns due to the lower resolution of the EIT flat-field. Off disk in the upper right corner, the ratio is slightly lower than the average. This can be due either to an excess of MXUVI signal or to a lack of EIT signal. But a close look at all the EIT images reveal a systematic asymmetry of the corona, the lower left and upper right corners of the 17.1 nm and 19.5 nm images being always brighter than the two other ones, and the contrary in the 30.4 nm and 28.4 nm images (see Figures 3 and 4). Since the MXUVI pupil is symmetric, we conclude that the dark region that we observe in the upper right corner of Figure 7(a) is due to an asymmetry of the stray-light function of the EIT. The cause of this asymmetry is still unknown but might be due to the polishing process of the mirrors of the EIT or the asymmetric support grid pattern in the foil mesh at the EIT pupil.

The 1998 ratio is strongly non-uniform. Here also the small features on the disk are due to the low resolution of the flat-field of EIT. The ratio rises continuously

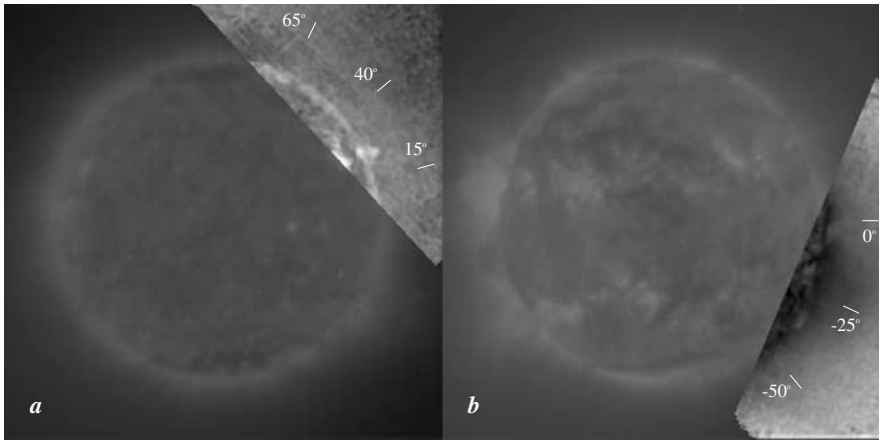

Figure 7. Ratios of the MXUVI and EIT images of 1997 (a) and 1998 (b). The corresponding EIT 17.1 nm images are displayed in background. The white ticks indicate the position of the radial cuts of Figure 8. Unlike the Figure 6 ratios, these maps are not functions of the EIT flat-field but reflect the ratio of the stray-light levels between the two instruments.

as we go higher above the limb and to the south. This means that the further from the limb, the higher the stray-light level in EIT compared to the stray-light level in the MXUVI. This behavior was expected since the MXUVI had a smoother mirror in 1998 than in 1997. We also observe the same effect as in 1997: the lower right corner is brighter because of the asymmetric stray-light function of the EIT. This behavior is well illustrated by the radial cuts of Figure 8 extracted at the angles defined by the white ticks in Figure 6. Since on disk the images are dominated by signal, we scaled the EIT and MXUVI images to match on disk. In 1997, the EIT and MXUVI curves are very similar, except at 40 degrees, revealing again the lower stray-light level in the EIT in this corner due to the asymmetry of the EIT stray-light function. In the 1998 profiles, it is obvious that the MXUVI had much less stray-light than EIT, with the signal falling off with a much steeper slope. If we assume that the MXUVI data of 1998 are free of stray-light, then the ratio (EIT – MXUVI)/EIT of the profiles of Figure 8 gives a lower limit for the percentage of the signal due to the stray-light in the 17.1 nm EIT images. Table I gives these values for three different heights above the limb. It is obvious that the stray-light level in the 17.1 nm images becomes non-negligible very rapidly, reaching about 50% at 1.5 solar radii. Higher in the corona, the signal becomes dominated by the stray light. Further analysis has to be done in order to obtain an operational stray-light subtraction.

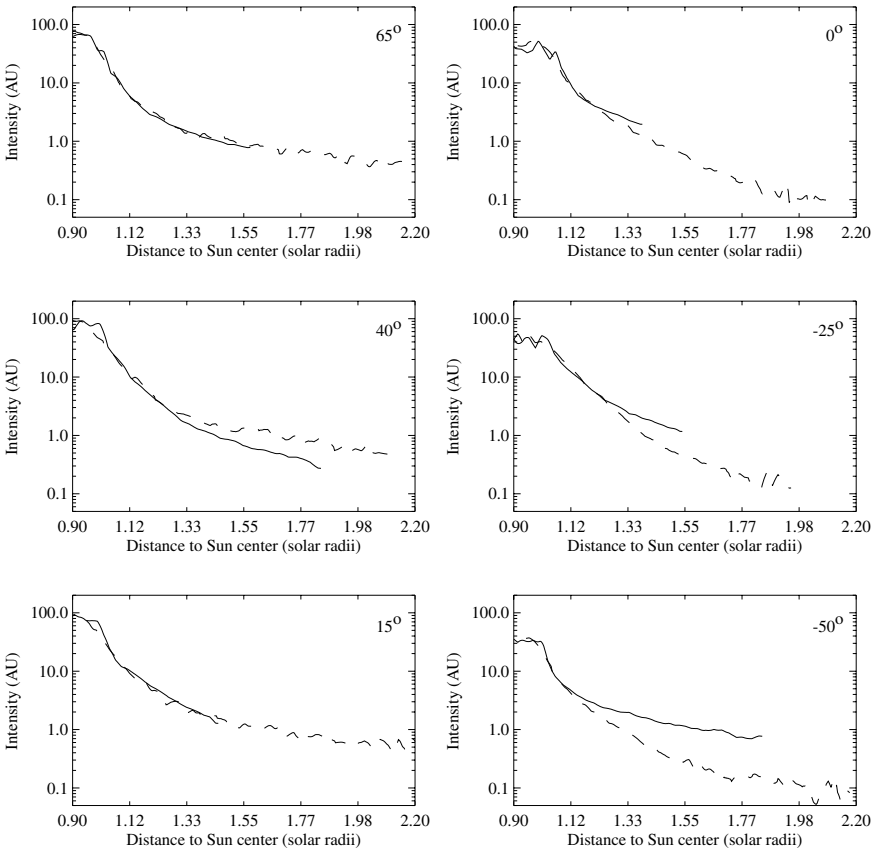

Figure 8. Radial profiles across the MXUVI (*dashed lines*) and EIT (*solid lines*) images of 1997 (*left*) and 1998 (*right*) at the angles indicated in Figure 7 by white dashes. Angles are ordered counterclockwise, with the origin at the west equator. The asymmetry of the stray-light function of the EIT is obvious in the 1997 cut at 40 deg. In 1998, due to a smoother mirror, the MXUVI had a much lower stray-light level than EIT at all angles.

TABLE I

Estimated stray-light level in the 17.1 nm EIT images at three different heights above the limb.

Position angle (deg)	Stray light level		
	1.1 $R_\odot$	1.4 $R_\odot$	1.8 $R_\odot$
0	$\leq 5\%$	30%	–
−25	$\leq 5\%$	45%	–
−50	$\leq 5\%$	60%	80%

4. Conclusions

The EIT instrument on board SOHO suffers from a lack of pre-flight calibration of the stray light. In addition, because of the degradation of its detector, its response varies with time. The two sounding rocket flights of the MXUVI instrument on 15 May 1997 and 2 November 1998 provided data of good quality for inter-calibration purposes with the EIT instrument. These observations, made one and a half years apart, allowed us to evaluate the evolution of the EIT response over this period of time. Flat-fields of the EIT CCD have been extracted that can help constrain the aging models, which are still under development. Evaluating the stray-light level is a very important issue when analyzing EIT coronal observations, because in some cases the signal can become stray-light dominated. In that sense, the MXUVI observations have led to crucial improvements, especially by giving the first estimates of the stray-light level in the EIT images and by showing the asymmetry of the stray-light function of the EIT. This aspect is still under study to obtain an operational stray-light subtraction. The 1998 flight also showed that stray-light levels significantly lower than in the EIT can be achieved with the state-of-the-art superpolishing and multi-layer technology. This result encourages the development of even lower scattering optics for future XUV coronagraphs such as the SOPHIE (Hassler *et al.*, 1998) project.

Acknowledgements

The success of these rocket flights is due in large part to the dedicated efforts of many people. In particular, Bill Tomlinson at SwRI and Greg Ucker at LASP were essential to the success of this program. We would also like to thank the staff of the Research Rockets Division of the White Sands Missile Range, the SPARCS Division of Lockheed-Martin and the personnel of the Physical Sciences Laboratory of New Mexico State University for their untiring support. We would also like to thank Jean-Pierre Chauvineau at the Institut d'Optique in Orsay, France and Troy Barbee at Lawrence Livermore National Laboratory for providing the multi-layer coatings for our 1997 and 1998 flights, respectively. We also thank Jean-Pierre Delaboudinière for useful discussions and scientific support, as well as acknowledgment of his essential contribution as PI of the EIT instrument on SOHO. SOHO is a project of international cooperation between ESA and NASA. EIT images are courtesy of the SOHO/EIT consortium. A portion of the work of DMH has been supported by NASA under grant NAG5-5140 to Southwest Research Institute.

References

Auchère, F., DeForest, C. E., and Artzner, G.: 2000, *Astrophys. J.* **529**, 115.
Defise, J.-M., Moses, J. D., and Clette, F.: 1998, *Proc. SPIE* **3442**, 126.
Defise, J.-M., Clette, F., Moses, J. D., and Hochedez, J. F.: 1998, *Proc. SPIE* **3114**, 598.
Delaboudinière, J. P. *et al.*: 1995, *Solar Phys.* **162**, 291.
Dere, K. P. *et al.*: 2000, *Solar Phys.* **195**, 13.
Domingo, V., Fleck, B., and Poland, A. I.: 1995, *Solar Phys.* **162**, 1.
Hassler, D. M., Slater, D., Smartt, R., and Koutchmy, S.: 1998, *Proc. SPIE*, **3443** 61.
Moses J. D. *et al.*: 1997, *Solar Phys.* **175**, 571.
Newmark, J. S. *et al.*: 2000 *Proc. SPIE* **4139**, 328.